ISSN 2616-5880 Vol. 7, Issue 1: 73-79, DOI: 10.25236/AJMC.2026.070111

Darcy Flow Characteristics in Regular Pore-Throat Structures: A Microfluidic Experimental Study

Xinyi Zhang[1,a]

[1]*College of Science, China Jiliang University, Hangzhou, 310018, China*
[a]*p23080854036@cjlu.edu.cn*

Abstract: *Darcy flow behavior in porous media is of significant importance in engineering problems such as energy extraction and groundwater transport, with its macroscopic permeability characteristics largely controlled by the geometry of the pore throat structure. To quantitatively analyze the influence of regular pore throat structures on Darcy flow behavior and equivalent permeability, this study employs a microfluidic experimental method, selecting two types of chips with identical porosities but different pore throat geometries for comparative experiments. The permeability performance of these chips under Darcy flow conditions was then compared. By measuring the relationship between the pressure gradient and volumetric flow rate under steady-state conditions, the equivalent permeability of the two chips was calculated based on Darcy's law, thereby studying the impact of pore throat geometry on flow characteristics. The experimental results show that the permeabilities of the two chips are 2.083×10^{-8} m² and 4.16×10^{-8} m², respectively. Despite having similar porosities, the triangular pore throat chip exhibited a significantly higher permeability due to differences in geometric structure. During the experiment, bubble retention and local preferential flow phenomena were observed, but these did not disrupt the linear relationship of Darcy flow and only had a slight effect on the quantitative results of the equivalent permeability. This study reveals the influence of regular pore throat structures on Darcy flow characteristics in porous media through microfluidic experiments, providing experimental evidence for understanding and predicting macroscopic permeability based on pore-scale structures.*

Keywords: *Porous medium, Darcy flow, Microfluidics, Pore throat structure, Equivalent permeability*

1. Introduction

Flow in porous media is ubiquitous in energy extraction, groundwater transport, and environmental engineering. The macroscopic flow characteristics of porous media are fundamentally controlled by the microstructure of the pores[1]. Under low flow conditions, the flow of fluid in porous media is primarily governed by viscous resistance, and the process can be described by Darcy's law. This law provides a linear relationship between the flow rate and pressure gradient under steady-state laminar flow conditions in porous media[2]. The general form of Darcy's law is expressed as:

$$Q = A\frac{K}{\mu}\frac{\Delta P}{L} \tag{1}$$

Where Q is the volumetric flow rate, A is the cross-sectional area of the porous medium, μ is the dynamic viscosity of the fluid, K is the permeability of the porous medium, ΔP is the pressure difference across the medium, and L is the characteristic length of the flow. This equation indicates that under low-speed flow conditions, the flow rate and pressure gradient exhibit a linear relationship, and permeability is the key parameter that quantifies the flow capacity of the porous medium.

Experimental measurement is the most intuitive and effective method for studying the Darcy flow characteristics of porous media. Early studies focused on particle beds or natural rock samples, using macroscopic experimental techniques to establish empirical relationships between permeability and structural parameters. Lei et al. [3] derived an empirical formula for permeability based on particle bed experiments; Scholz et al. [4] measured the permeability of randomly packed elliptical particles, showing that permeability is primarily dependent on the overlap probability of particles rather than their shape. Jiang et al. [5] developed an empirical formula for the permeability of porous media using measurements of power-law fluids; Adler et al. [6] derived permeability expressions for glass particle media. For natural rock samples, Ehrenberg et al. [7] investigated the impact of porosity and pore throat diameter on the permeability of carbonate rocks, while Burgisser et al. [8] demonstrated the critical role of pore throat

ISSN 2616-5880 Vol. 7, Issue 1: 73-79, DOI: 10.25236/AJMC.2026.070111

structure in controlling magma flow in volcanic rocks. Baker et al. [9] discovered a power-law relationship between permeability and porosity in basalt. Additionally, studies by Rust [10], Klug [11], and Farquharson et al. [12] have shown that bubble structure, connectivity, pressure differences, and fluid viscosity significantly influence permeability.

Despite significant advancements in traditional experimental studies on Darcy flow laws, the impact of pore throat geometry on flow behavior remains challenging to directly observe and quantify due to the inherent randomness of natural pore structures. With the development of microfluidic technology, microfluidic experiments using artificially designed pore networks have provided new insights into the study of flow in porous media. Xu et al. [13] developed a microfluidic platform to observe the flow behavior of oil droplets in simulated pore throat structures and studied the role of nanoparticles in enhancing non-wetting phase displacement. Wang et al. [14, 15] used microfluidic experiments to visualize and quantify displacement processes in complex porous media and proposed a novel displacement model to enhance displacement efficiency in heterogeneous porous media.

In addition to the displacement process, microfluidic techniques have been widely applied to study pore-scale flow behaviors in porous media. Relevant studies include bubble growth and coalescence behaviors [16, 17], evaporation and salt precipitation processes [25], gas-liquid displacement and capillary instability [18], high-pressure multiphase flow [19], as well as multiphase flow, preferential flow, and imbibition processes [20–23]. Furthermore, microfluidic technology has been used for the quantitative measurement of interfacial properties at the pore scale, such as surface charge measurements at liquid-liquid interfaces [24]. These studies demonstrate the advantages of microfluidic experiments in visualizing and analyzing pore-scale flow mechanisms.

In summary, while microfluidic experiments have demonstrated high controllability and visualizability for studying pore-scale flow in porous media, experimental studies on Darcy flow characteristics and equivalent permeability in regular pore throat structures are still limited. Therefore, this study employs microfluidic experiments to investigate Darcy flow behavior in porous media with regular pore throat structures under low flow conditions. By analyzing the relationship between pressure gradient and volumetric flow rate, the equivalent permeability under different pore throat structures was quantitatively characterized. Additionally, the relationship between pore-scale flow features and macroscopic flow behavior in regular pore throat structures was explored, considering the bubble retention and local preferential flow phenomena observed during the experiment.

2. Experimental Method

2.1 Experimental Setup

The microfluidic experimental system used in this study consists primarily of microfluidic pore throat chips, a syringe pump, pressure sensors, and an optical microscopy system, as shown in Figure 1. The syringe pump is employed to inject fluid into the chip at a stable flow rate, while the pressure sensors monitor the pressure variations at both ends of the chip to determine the pressure gradient under steady-state conditions. The optical microscopy system is used to observe the flow behavior within the chip and pore-scale phenomena.

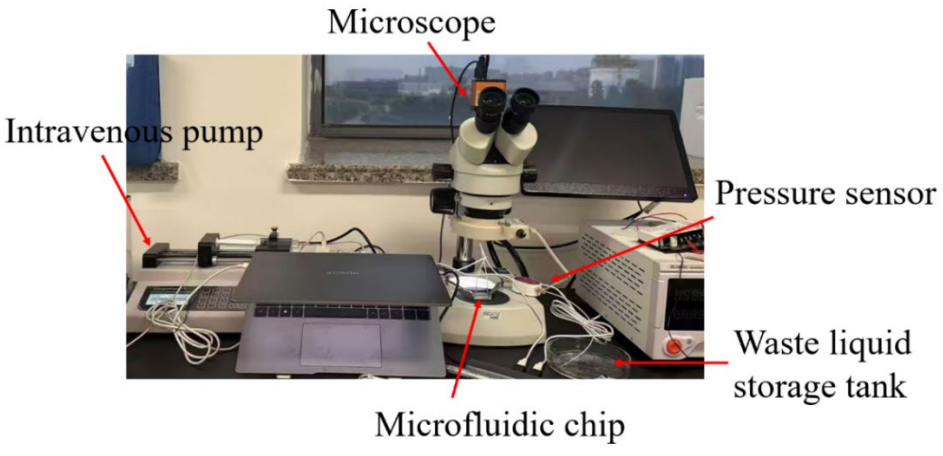

Figure 1: Schematic of the experimental setup and testing system

ISSN 2616-5880 Vol. 7, Issue 1: 73-79, DOI: 10.25236/AJMC.2026.070111

The fluid used in the experiments is deionized water, which serves as the single-phase fluid for the displacement process. To minimize the effects of dissolved gases on experimental results, the deionized water is degassed for 30 minutes before use. The entire setup operates at room temperature, with an ambient temperature of approximately 20°C to ensure consistent experimental conditions.

2.2 Microfluidic Chips

The microfluidic chips used in this study are fabricated from polydimethylsiloxane (PDMS) through soft lithography, and bonded to glass substrates using plasma treatment to form enclosed flow channels. The chips are designed with inlet and outlet ports for connecting external injection and measurement devices.

The pore throat chips selected for the experiment are square-shaped and triangular-shaped, as shown in Figure 2. The chip dimensions are specified as follows: length $l = 20\text{mm}$, width $W = 10\text{mm}$, and depth $H = 0.1mm$, with cylindrical micro-pillars designed $d = 0.2mm$ inside the chip having diameters and depths. The square-shaped pore throat chip has a porosity of 0.68905, a center-to-center spacing of 0.3 mm, and a micro-pillar angle of 0°; the triangular-shaped pore throat chip has the same porosity as the square-shaped chip, with a center-to-center spacing of 0.3 mm and a micro-pillar angle of 10°. Based on these pore throat chips, this study adjusts the pore throat geometric structure to investigate the impact of pore throat morphology differences on Darcy flow characteristics.

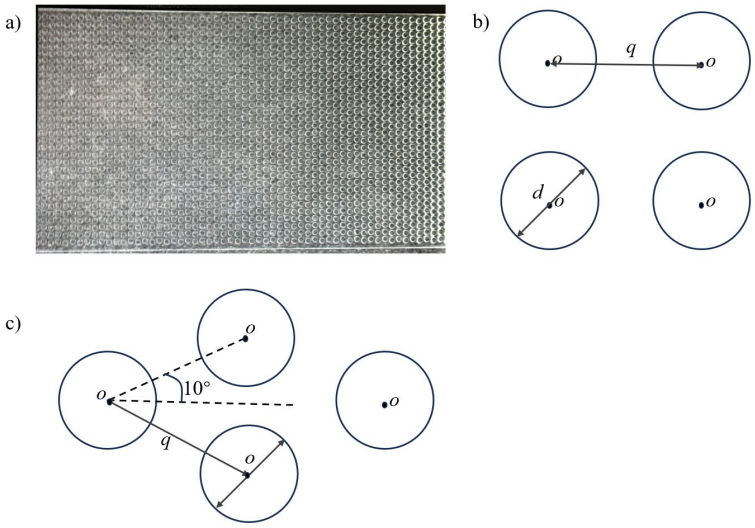

(a)Physical image of triangular chip; (b) Schematic diagram of square chip; (c) Schematic diagram of triangular chip

Figure 2: Schematic diagram of microfluidic pore-chip structure

2.3 Experimental Procedure

The experimental procedure consists of the following main steps: preparing degassed water, saturating the chip, and performing the flow tests.

Before starting the experiment, the deionized water is placed in a vacuum chamber for 30 minutes to remove dissolved gases. After assembling the experimental system and calibrating the pressure sensors, the chip is injected with degassed water at a high flow rate (1000 μL/min) to remove air bubbles. The chip is observed under a microscope to ensure it is free from visible air bubbles before it is considered saturated.

Once the chip is saturated, the flow rate is gradually decreased to 100 μL/min, and degassed water is continuously injected. The pressure sensor readings are monitored until they stabilize, and the corresponding pressure values are recorded. Afterward, the flow rate is increased incrementally to 2000 μL/min, and for each new flow rate, the system is allowed to stabilize before recording the pressure values. The entire procedure is repeated three times for each type of pore throat chip, and the average of these measurements is used for further analysis.

ISSN 2616-5880 Vol. 7, Issue 1: 73-79, DOI: 10.25236/AJMC.2026.070111

3. Results and Discussion

3.1 Darcy Permeability Fitting

Under low flow conditions, microfluidic experiments were conducted to compare the flow behavior of the square-shaped pore throat chip and the triangular-shaped pore throat chip. The experimental results demonstrate that, within the studied flow range, the pressure gradient and flow rate for both the square-shaped and triangular-shaped chips exhibit a good linear relationship (as shown in Figure 3), which aligns with the basic assumption of Darcy's law.

By performing linear fitting on the pressure gradient and volumetric flow rate data, the equivalent permeability for each chip was obtained, as shown in Table 1. The results reveal that the equivalent permeability of the square-shaped chip is 2.083×10^{-8} m², while the equivalent permeability of the triangular-shaped chip is 4.16×10^{-8} m². The permeability of the triangular-shaped pore throat chip is significantly higher than that of the square-shaped pore throat chip. This difference indicates that, despite having the same porosity, the distinct pore throat geometries exert a substantial impact on permeability performance.

As the micro-pillar angle increases, the guiding effect on flow lines is enhanced, reducing local flow resistance and thereby increasing permeability. This phenomenon is closely related to the flow characteristics of fluids in different pore geometries, where the triangular pore throat geometry facilitates smoother fluid flow, reducing local energy dissipation.

Table 1: Equivalent Permeability of Chips with Different Pore-Channel Structures

Chip type	Fit slope	Darcy permeabilitym^2	R^2
Square-shaped chip	0.481	2.083×10^{-8}	0.99
Triangular-shaped chip	0.241	4.16×10^{-8}	0.99

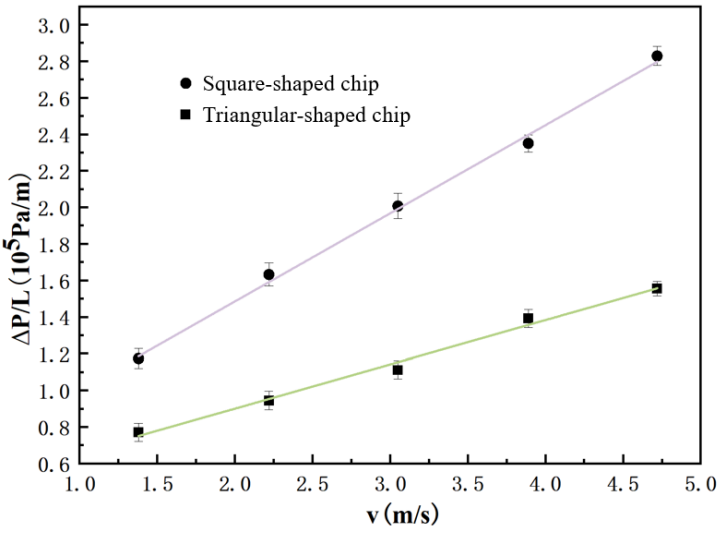

Figure 3: Relationship between pressure gradient and flow rate in chips with different pore and throat structures

3.2 Pore-Scale Characteristics of Bubble Retention and Preferential Flow Phenomena

During the experiment, although the chips were thoroughly degassed prior to the flow testing, bubble retention phenomena were still observed in certain pore throat regions, particularly at locations of pore throat contraction and areas with local geometric discontinuities. As shown in Figure 4, the presence of bubbles occupies part of the effective flow path, altering the surrounding streamlines and thereby impacting local flow resistance.

ISSN 2616-5880 Vol. 7, Issue 1: 73-79, DOI: 10.25236/AJMC.2026.070111

Figure 4: shows a schematic of the bubbles within the chip (square pore throat chip, 10 μL/min).

The presence of bubbles modifies the effective cross-sectional flow area of the local pore throat, introducing additional flow resistance at the pore scale. When a bubble occupies part of the pore throat space, the fluid is forced to bypass the bubble through the remaining channel, causing changes in the local velocity distribution. On the macroscopic scale, this localized blockage effect does not disrupt the overall linear relationship between pressure difference and flow rate, but may influence the quantitative value of the equivalent permeability.

In addition, clear preferential flow phenomena were observed in some pore throat structures, as shown in Figure 5. Microscopic observations reveal that in a regular pore throat network, fluid does not flow uniformly through all the pores, but instead tends to preferentially flow along continuous pathways with lower resistance, forming a stable primary flow channel.

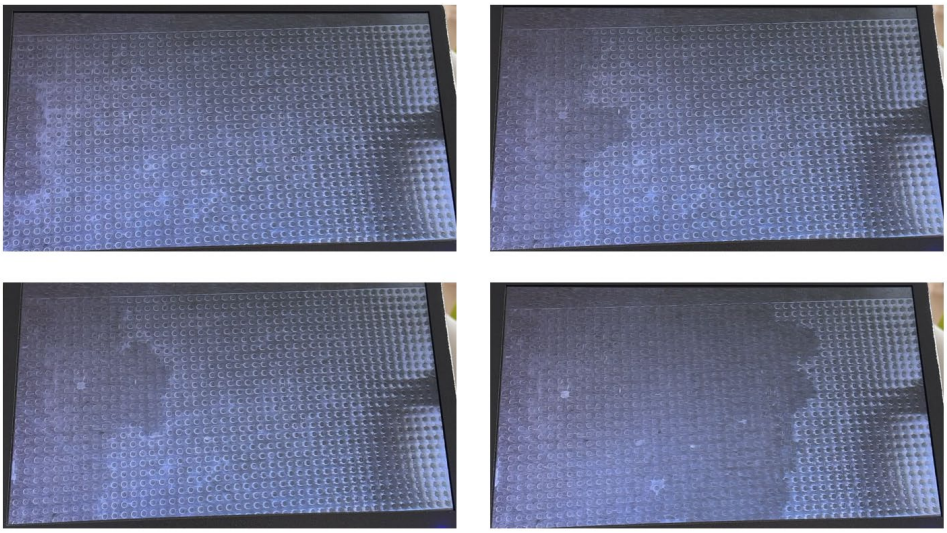

Figure 5: Illustrates the preferential flow phenomenon (square pore throat chip, 20 μL/min).

From a physical mechanism perspective, both bubble retention and preferential flow phenomena result from the modulation of local flow by the pore throat geometry. The inhomogeneity at the pore throat scale, as well as local geometric constraints, amplify the impact of small disturbances on flow path selection, leading to non-uniform flow distribution at the pore scale. It is important to note that within the low flow rate range studied in this work, these pore-scale phenomena do not cause failure of Darcy's law, but rather affect the measurement of equivalent permeability by altering the local flow structure.

4. Conclusion

This study, based on microfluidic experimental methods, investigates the Darcy flow characteristics and equivalent permeability of square-shaped and triangular-shaped pore throat chips under low flow conditions. The following main conclusions were drawn by comparing the permeability of the two pore

ISSN 2616-5880 Vol. 7, Issue 1: 73-79, DOI: 10.25236/AJMC.2026.070111

throat structures:

(1) The square-shaped and triangular-shaped pore throat chips, with the same porosity, exhibit significant differences in permeability. The equivalent permeability of the triangular-shaped pore throat chip is 4.16×10^{-8} m², which is higher than that of the square-shaped pore throat chip (2.083×10^{-8} m²). This difference is primarily attributed to the geometric disparity between the two pore throat structures, where the geometric optimization of the triangular pore throat reduces local flow resistance and enhances permeability performance.

(2) Both pore throat structures exhibit a good linear relationship between pressure gradient and flow rate within the experimental flow range, consistent with the basic assumptions of Darcy's law. The experimental results show that the flow process remains under low Reynolds number conditions, with no noticeable inertial effects observed.

(3) Although bubble retention and preferential flow phenomena were observed during the experiment, these pore-scale effects had a minimal impact on the linear relationship of the overall Darcy flow behavior, only slightly affecting the quantitative results of equivalent permeability.

This study provides experimental evidence for the investigation of flow characteristics in porous media using microfluidic experiments and offers insights for further optimization of pore structure to improve the accuracy of permeability measurements. More broadly, this work demonstrates the utility of microfluidic experiments as a versatile tool for investigating pore-scale transport phenomena, with potential applications extending from geoscience to biomedical engineering and materials design.

References

[1] Yu B. Analysis of flow in fractal porous media[J]. Applied Mechanics Reviews, 2008, 61(5): 050801.
[2] Montiel D. Darcy H (translated by Bobeck P): The public fountains of the city of Dijon[J]. Environmental Earth Sciences, 2013, 70(6): 2929–2930.
[3] Lei, S. Y., Wang, L. Q., Jia, L. Q., et al. Relationship between porosity and permeability of granular beds[J]. Journal of Tsinghua University, 1998, 38(5), 20–28.
[4] Scholz C, Wirner F, Goetz J, et al. Permeability of porous materials determined from the Euler characteristic[J]. Physical Review Letters, 2012, 109(26): 264504.
[5] Jiang, T. Q., Fang, T. N., & Chen, G. H. Study on rheological properties of power-law fluids[J]. Journal of East China Institute of Chemical Technology, 1982, 1, 28–37.
[6] Adler P M. Transport processes in fractals—I. Conductivity and permeability of a Leibniz packing in the lubrication limit[J]. International Journal of Multiphase Flow, 1985, 11(1): 91–108.
[7] Ehrenberg S, Nadeau P H. Sandstone vs. carbonate petroleum reservoirs: A global perspective on porosity–depth and porosity–permeability relationships[J]. AAPG Bulletin, 2005, 89(4): 435–445.
[8] Burgisser A, Gardner J E, et al. The percolation threshold and permeability evolution of ascending magmas[J]. Earth and Planetary Science Letters, 2017, 470: 37–47.
[9] Baker D R, Brun F, Mancini L, et al. The importance of pore throats in controlling the permeability of magmatic foams[J]. Bulletin of Volcanology, 2019, 81(9): 2–17.
[10] Rust A C, Cashman K V. Permeability of vesicular silicic magma: Inertial and hysteresis effects[J]. Earth and Planetary Science Letters, 2004, 228: 93–107.
[11] Klug C, Cashman K V. Permeability development in vesiculating magmas: Implications for fragmentation[J]. Bulletin of Volcanology, 1996, 58: 87–100.
[12] Farquharson J, Heap M J, Varley N R, et al. Permeability and porosity relationships of edifice-forming andesite lavas: A combined field and laboratory study[J]. Journal of Volcanology and Geothermal Research, 2015, 297: 52–68.
[13] Xu K, Zhu P, Huh C, et al. Microfluidic investigation of nanoparticles' role in mobilizing trapped oil droplets in porous media[J]. Langmuir, 2015, 31(51): 14004–14012.
[14] Lei W, Lu X, Wu T, et al. High-performance displacement by microgel-in-oil suspension in heterogeneous porous media: Microscale visualization and quantification[J]. Journal of Colloid and Interface Science, 2022, 627: 1–13.
[15] Lu X, Wang M. High-performance nanogel-in-oils as emulsion evolution controller for displacement enhancement in porous media[J]. ACS Applied Materials & Interfaces, 2023, 15(42): 48963–48975.
[16] Xu K, Ge X H, Huang J P, et al. A region-selective modified capillary microfluidic device for fabricating water–oil Janus droplets and hydrophilic–hydrophobic anisotropic microparticles[J]. RSC Advances, 2015, 5: 46981–46988.

ISSN 2616-5880 Vol. 7, Issue 1: 73-79, DOI: 10.25236/AJMC.2026.070111

[17] Zhang, Y. N., Wang, J. Q., Feng, Z., et al. Growth and coalescence behavior of bubbles in porous media under heating conditions[J]. CIESC Journal, 2023, 74(4), 1–12.
[18] Zhang T, Wu R, Zhao C Y, et al. Capillary instability induced gas–liquid displacement in porous media: Experimental observation and pore network model[J]. Physical Review Fluids, 2020, 5(10): 104305.
[19] Zhang J, Yin Z, Khan S A, et al. Path-dependent morphology of CH_4 hydrates and their dissociation studied with high-pressure microfluidics[J]. Lab on a Chip, 2024, 24(6): 1–12.
[20] Lei W, Li Q, Yang H E, et al. Preferential flow control in heterogeneous porous media by concentration-manipulated rheology of microgel particle suspension[J]. Journal of Petroleum Science and Engineering, 2023, 212: 110275.
[21] Lu X, Wang M. Shape and surface property effects on displacement enhancement by nanoparticles[J]. International Journal of Mechanical Sciences, 2023, 255: 108471.
[22] Lei W, Lu X, Liu F, et al. Non-monotonic wettability effects on displacement in heterogeneous porous media[J]. Journal of Fluid Mechanics, 2022, 942: A12.
[23] Lei W, Lu X, Gong W, et al. Triggering interfacial instabilities during forced imbibition by adjusting the aspect ratio in depth-variable microfluidic porous media[J]. Proceedings of the National Academy of Sciences, 2023, 120(50): e2307455120.
[24] Alizadeh A, Huang Y, Liu F, et al. A streaming-potential-based microfluidic measurement of surface charge at immiscible liquid–liquid interface[J]. International Journal of Mechanical Sciences, 2023, 247: 108200.
[25] Wu R, Chen F. Interplay between salt precipitation, corner liquid film flow, and gas–liquid displacement during evaporation in microfluidic pore networks[J]. Journal of Applied Physics, 2023, 133: 074701.